



JOURNAL OF
APPLIED
CRYSTALLOGRAPHY

Volume 55 (2022)

Supporting information for article:

Co-flow injection for serial crystallography at X-ray free-electron lasers

Diandra Doppler, Mohammad T. Rabbani, Romain Letrun, Jorvani Cruz Villarreal, Dai Hyun Kim, Sahir Gandhi, Ana Egatz-Gomez, Mukul Sonker, Joe Chen, Faisal H. M. Koua, Jayhow Yang, Mohamed Youssef, Victoria Mazalova, Saša Bajt, Megan L. Shelby, Matt A. Coleman, Max O. Wiedorn, Juraj Knoska, Silvan Schön, Tokushi Sato, Mark S. Hunter, Ahmad Hosseinizadeh, Christopher Kuptiz, Reza Nazari, Roberto C. Alvarez, Konstantinos Karpos, Sahba Zaare, Zachary Dobson, Erin Discianno, Shangji Zhang, James D. Zook, Johan Bielecki, Raphael de Wijn, Adam R. Round, Patrik Vagovic, Marco Kloos, Mohammad Vakili, Gihan K. Ketawala, Natasha E. Stander, Tien L. Olson, Katherine Morin, Jyotirmoy Mondal, Jonathan Nguyen, José Domingo Meza-Aguilar, Gerdenis Kodis, Sara Vaiana, Jose M. Martin-Garcia, Valerio Mariani, Peter Schwander, Marius Schmidt, Marc Messerschmidt, Abbas Ourmazd, Nadia Zatsepin, Uwe Weierstall, Barry D. Bruce, Adrian P. Mancuso, Thomas Grant, Anton Barty, Henry N. Chapman, Matthias Frank, Raimund Fromme, John C. H. Spence, Sabine Botha, Petra Fromme, Richard A. Kirian and Alexandra Ros

1. Numerical Modeling.

To simulate the co-flow width, the laminar two-phase flow and Level Set Method (LSM) are used. “Fine” meshing was selected during the simulation, which created a domain of 696196 triangular elements, 24102 boundaries, and 792 edges, respectively. Walls are considered as wetted and impermeable. More detailed boundary conditions, their relevant equations, and nomenclature used in the two-phase flow and level set method are described in Table S1. The parameters used in the model are listed in Table S2.

2D Model.

A 2D model matching the cross-section of the co-flow devices in the experimental observation plane was set up first. The result of numerical modeling is shown for co-flow in three different flow conditions in the T-junction and Y-junction in Figure S1.

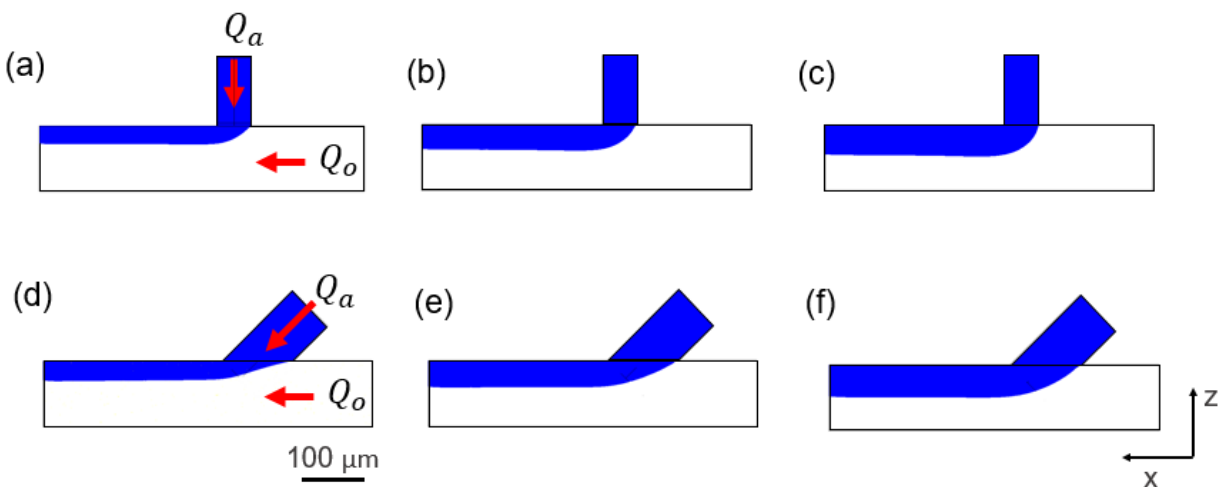


Figure S-1. Result of numerical modeling for co-flow of different flow conditions in T- and Y-junction for Mode 1: The flow rates are a) $Q_o = 18 \mu\text{L}/\text{min}$ and $Q_a = 2 \mu\text{L}/\text{min}$, b) $Q_o = 16 \mu\text{L}/\text{min}$ and $Q_a = 4 \mu\text{L}/\text{min}$, c) $Q_o = 14 \mu\text{L}/\text{min}$ and $Q_a = 6 \mu\text{L}/\text{min}$, d) $Q_o = 18 \mu\text{L}/\text{min}$ and $Q_a = 2 \mu\text{L}/\text{min}$, e) $Q_o = 16 \mu\text{L}/\text{min}$ and $Q_a = 4 \mu\text{L}/\text{min}$, and f) $Q_o = 14 \mu\text{L}/\text{min}$ and $Q_a = 6 \mu\text{L}/\text{min}$. The average co-flow thickness of each conditions are a) $18.12 \pm 0.65 \mu\text{m}$, b) $27.16 \pm 0.89 \mu\text{m}$, c) $38.66 \pm 1.31 \mu\text{m}$, d) 32.88 ± 0.56 , e) 49.35 ± 0.89 , and f) 52.31 ± 1.36 respectively. The blue color represents the aqueous sample phase. The oil phase is presented in white in the continuous channel.

3D Model.

To illustrate the curved nature of the water/oil interface, a 3D model was established. Briefly, a 3D model of the T-junction was established to reflect the 3D-printed device investigated in this work, as shown in Figure S-2. The T-junction design consists of a cylindrical tube with an inner diameter of $75 \mu\text{m}$, connected to the rectangular fluidic channel. The height, width, and length of the rectangular channel are 100 , 100 , and $500 \mu\text{m}$, respectively. To simulate the co-flow, laminar two-phase incompressible flow and the Level Set Method (LSM) were used. Meshing was chosen as “fine,” and walls are considered wetted and impermeable. More detailed boundary conditions, other relevant equations, and nomenclature used in the two-phase flow and level set method are described below in Table S-1.

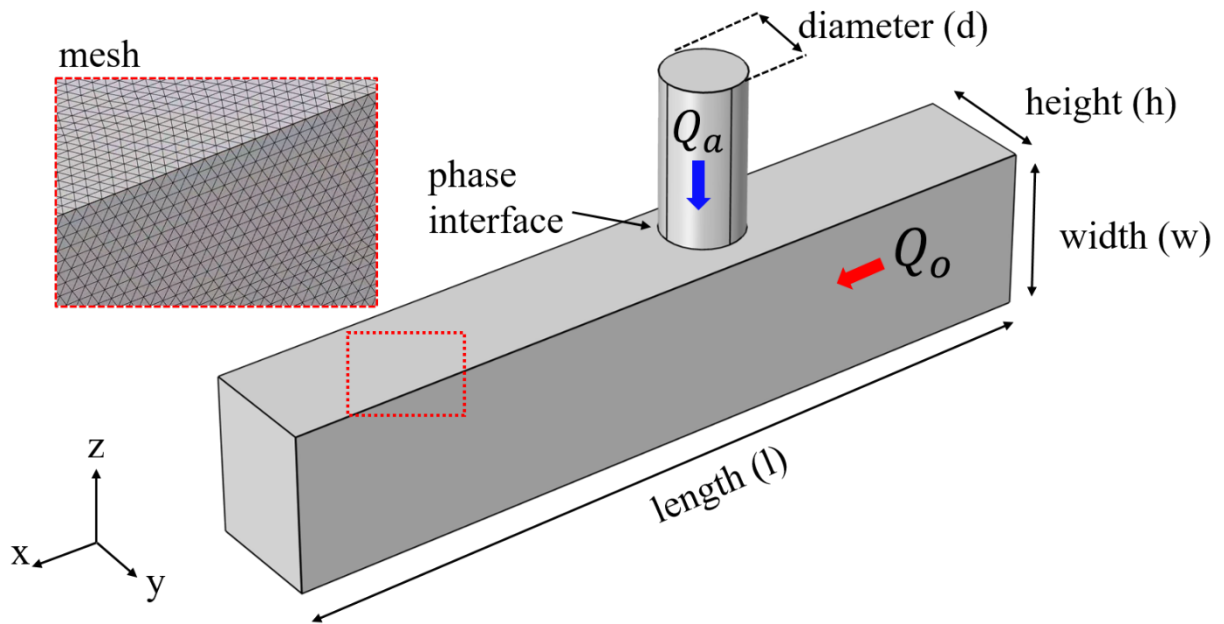


Figure S-2. Schematic of the T-junction microchannel in the numerical study. The main horizontal channel contains the continuous phase (Q_o , oil). The perpendicular inlet channel contains the aqueous phase (Q_a , buffer).

The 3D numerical modeling was carried out for co-flow in three different contact angle conditions is described in Figure S3 from the T-junction 3D model. The numerical simulation was performed at different oil flow (Q_o) and aqueous flow (Q_a) rates while maintaining a total flowrate, Q_{tot} , of 20 $\mu\text{L}/\text{min}$. We explored the simulation for a hydrophobic condition ($\theta = 143^\circ$) and a hydrophilic condition ($\theta = 71^\circ$). Figure S-3a) represents the oil/aqueous interface for the hydrophilic condition at a flow rate ratio of 1. The oil/interface is curved due to its hydrophilicity and is represented in figure S-3b). Figure S-3c) represents the oil/aqueous interface for the hydrophobic condition at a flow rate ratio of 1. Figure S-3-d) shows the curvature of this interface through the channel. For a flow rate ratio of 1.5 and higher, no co-flow was observed for the hydrophobic condition, and instead of the co-flow droplet generation was observed. Figure S-3e) represents the generation of droplets for $\theta = 143^\circ$ and a flow rate ratio of 1.5.

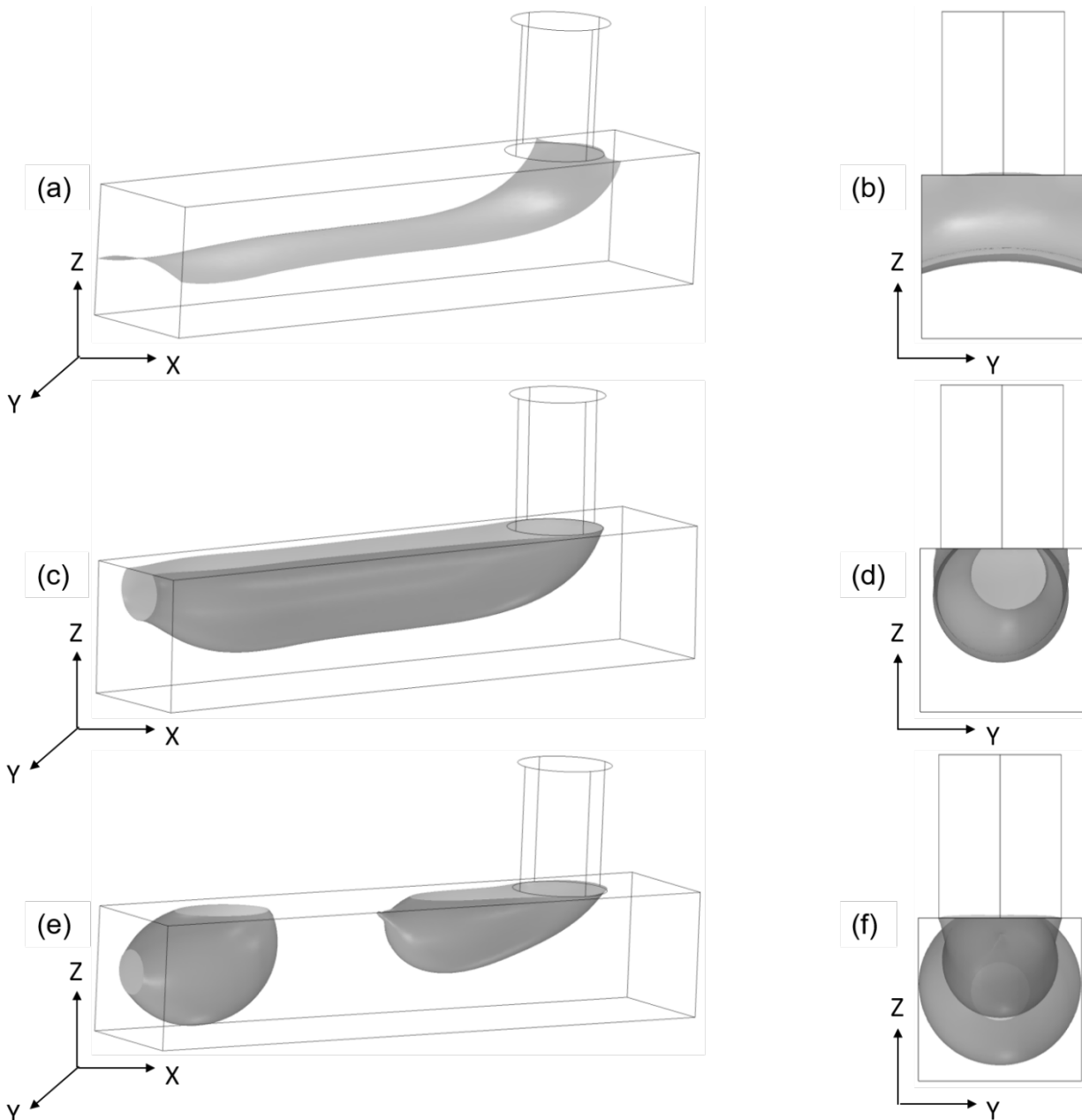


Figure S-3. Result of the oil/aqueous interface for a hydrophobic and hydrophilic condition at different flow rate ratios in a T-junction microchannel from the 3D numerical model. a) 3D-view of the oil/aqueous interface for ($\theta = 71^\circ$) with a flow rate ratio of 1. b) The view of the oil/aqueous interface when observed along the channel axis for conditions similar to a). c) The 3D-view of the oil/aqueous interface for ($\theta = 143^\circ$) with a flow rate ratio of 1. d) The view of the oil/aqueous interface along the channel axis for conditions similar to c). e) The generation of the droplet is observed for ($\theta = 143^\circ$) with a flow rate ratio of 3. f) The view of the oil/aqueous interface along the channel axis for conditions similar to e). Note that under this condition, the co-flow breaks into droplets.

Physics	Boundary conditions
Laminar Flow	<p>Surface domain: $0 = -\nabla p + \mu \nabla^2 \mathbf{u}$ $\rho \nabla \cdot (\mathbf{u}) = 0$ Wall : $u = 0$ (No slip condition) Inlets : Boundary condition = Laminar inflow (flow rate) Entrance thickness: $L_{\text{entr}} = 100 \mu\text{m}$ Outlet : $p_0 = 0$</p>
Level Set	<p>Surface domain (Phase initialization) : $\frac{\partial \phi}{\partial t} + \mathbf{u} \cdot \nabla \phi = \gamma \nabla \cdot \left(\varepsilon \nabla \phi - \phi(1 - \phi) \frac{\partial \phi}{ \nabla \phi } \right)$ Initial Value and Inlet for the oil phase: $\phi = 0$ Initial Value and Inlet for the aqueous phase: $\phi = 1$ γ: 0.0236 [N/m] * η_{oil} : 13.3 cP** η_{buffer} : 16.4 cP*** ρ_{oil}: density of oil: 1.8 [g/cm³] ρ_{buffer} : density of the buffer : 1.01 [g/cm³] Wetted wall: θ : 1.23 [rad] for the IP-S and 1.06 [rad] for the PETA-B-based resist</p>
Nomenclature	<p>ϕ = level set function γ = surface tension [mN/m] n = normal unit vector \mathbf{u} = medium or fluid velocity vector ρ_{oil}: density of PFD: PFO 10/1 v/v [g/cm³] ρ_{buffer} = density of the buffer [g/cm³] η_{oil} = viscosity of a PFD: PFO 10/1 v/v [cP] η_{buffer} = viscosity of buffer [cP] t = time [s] p = pressure [Pa] T = the absolute fluid temperature [K] u = fluid velocity [m/s] μ = dynamic fluid viscosity [Pa·s] θ = contact angle [rad]</p>

Table S-1. The boundary conditions for the simulation, relevant equations, and nomenclature. * from Echelmeier, A., *Sample Delivery Enabled by 3D Printing for Reduced Sample Consumption and Mix-and-Inject Serial Crystallography at X-ray Free Electron Lasers*, Thesis, Arizona State University, 2019. ** from Echelmeier et al. *Segmented Flow Generator for Serial Crystallography at X-Ray Free Electron Lasers*,

*Nature Communications, (2020) 11, 4511. *** Determined with the PSII buffer as defined in the main manuscript with a viscosimeter (DV1 Digital Viscometer, Brookfield Metek, USA)*

Flow rate ($Q_0: Q_a$) $\mu\text{l}/\text{min}$	ε (interface thickness) μm	γ (reinitialization parameter) m/s
19:1	0.73	0.032
18:2	0.73	0.030
16:4	0.73	0.028
15:5	0.73	0.025
14:6	0.73	0.030
12:8	0.73	0.037
10:10	0.73	0.047

Table S-2. Relevant simulation parameters used in the model.

2. Contact Angle Variation of 3D-printed Devices.

The sessile drop method was employed to measure the contact angle, θ , for the oil, water, 3D-printed surface system. The solid interface was made by 3D-printing a 5.0 mm x 5.0 mm x 0.1 mm block of either IP-S or PETA-B on a slide. A 5 μL droplet of water was placed on the polymer surface and the two were inverted and placed on top of a plastic cuvette overfilled with oil. A Jiusion USB Digital Microscope (Amazon, USA) connected to a laptop was used to capture the interface which was illuminated by a cell phone flash-light. The image of the interface (see Figure S-4 as an example) was analyzed in ImageJ¹ with the contact angle plug-in (<https://imagej.nih.gov/ij/plugins/contact-angle.html>) using the manual points procedure. Various times were assessed as shown in Figure S-5 and each timepoint was repeated in triplicate.

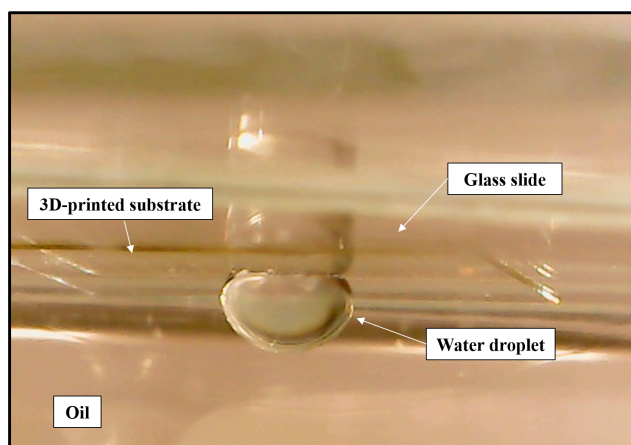


Figure S-4: Microscopic image of a 5 μL water droplet surrounded by oil on a 1- day old 3D-printed IP-S surface.

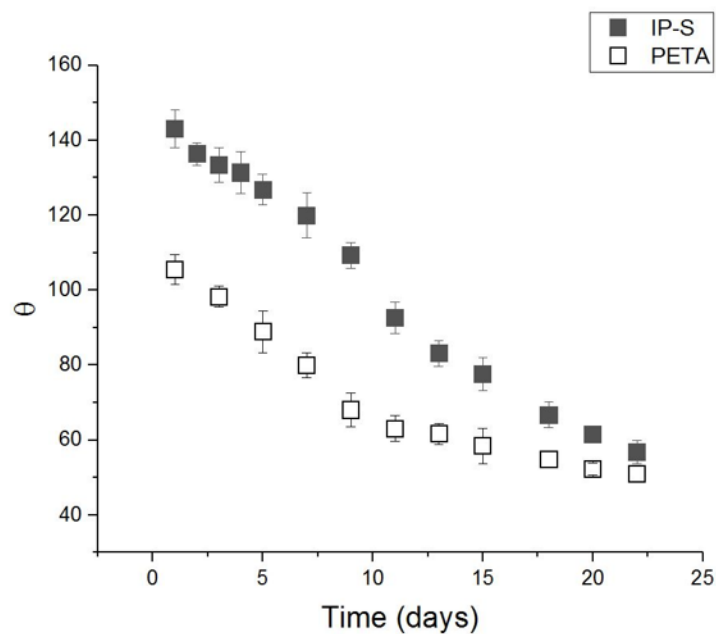


Figure S-5. Contact angle (θ) variation over time after device fabrication through 3D-printing both for resin IP-S and PETA-B.

3. Photosystem II crystals.

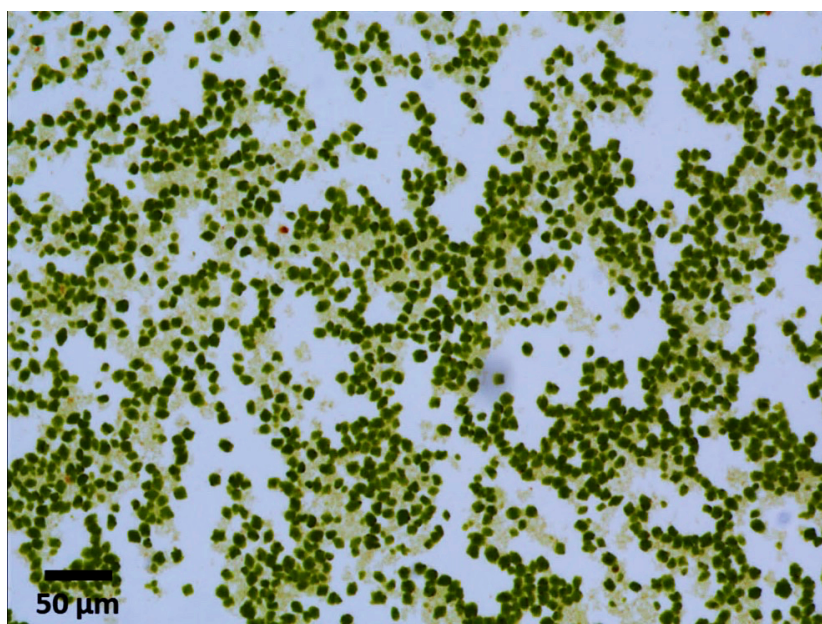


Figure S-6: Exemplary microscopy image of Photosystem II crystals grown in dehydration buffer.

References

1. Schneider, C. A.; Rasband, W. S.; Eliceiri, K. W., NIH Image to ImageJ: 25 years of image analysis. *Nat Methods* **2012**, 9 (7), 671-5.